

# Analysis on an improved resistance tuning type multi-frequency piezoelectric spherical transducer

Lei Qin<sup>1</sup>, Jianjun Wang<sup>\*\*2</sup>, Donghuan Liu<sup>2</sup>, Lihua Tang<sup>3</sup> and Gangbing Song<sup>\*4</sup>

<sup>1</sup>Research Center of Sensor Technology, Beijing Information Science & Technology University, Beijing 100192, P. R. China

<sup>2</sup>Department of Applied Mechanics, University of Science and Technology Beijing, Beijing 100083, P. R. China

<sup>3</sup>Department of Mechanical Engineering, University of Auckland, 20 Symonds Street, Auckland 1010, New Zealand

<sup>4</sup>Department of Mechanical Engineering, University of Houston, Houston, TX 77204, USA

(Received March 11, 2019, Revised April 24, 2019, Accepted April 25, 2019)

**Abstract.** The existing piezoelectric spherical transducers with fixed prescribed dynamic characteristics limit their application in scenarios with multi-frequency or frequency variation requirement. To address this issue, this work proposes an improved design of piezoelectric spherical transducers using the resistance tuning method. Two piezoceramic shells are the functional elements with one for actuation and the other for tuning through the variation of load resistance. The theoretical model of the proposed design is given based on our previous work. The effects of the resistance, the middle surface radius and the thickness of the epoxy adhesive layer on the dynamic characteristics of the transducer are explored by numerical analysis. The numerical results show that the multi-frequency characteristics of the transducer can be obtained by tuning the resistance, and its electromechanical coupling coefficient can be optimized by a matching resistance. The proposed design and derived theoretical solution are validated by comparing with the literature given special examples as well as an experimental study. The present study demonstrates the feasibility of using the proposed design to realize the multi-frequency characteristics, which is helpful to improve the performance of piezoelectric spherical transducers used in underwater acoustic detection, hydrophones, and the spherical smart aggregate (SSA) used in civil structural health monitoring, enhancing their operation at the multiple working frequencies to meet different application requirements.

**Keywords:** piezoelectric spherical transducer; spherical smart aggregate (SSA); piezoelectricity; multi-frequency characteristics; structural health monitoring

## 1. Introduction

Piezoelectric ultrasonic transducers with the unique feature of both sensing and actuating capacities (Agrawal *et al.* 1997, Meyer *et al.* 1998) have been designed in multiple structural forms for various engineering applications. These applications include acoustic pressure measurements in liquids (Lewin and Chivers 1981), compactness monitoring of concrete structure (Hou *et al.* 2018, Xu *et al.* 2018a, Luo *et al.* 2016), stress monitoring of concrete structure (Zhang *et al.* 2018, Du *et al.* 2017), water seepage monitoring in concrete (Liu *et al.*, 2013; Zou *et al.* 2014), metal corrosion and pipeline monitoring (Li *et al.* 2019, Du *et al.* 2016, Zhu *et al.* 2017), real-time evaluation of concrete cracks (Feng *et al.* 2018, Xu *et al.* 2018b), and health monitoring of concrete structures (Dumoulin and Deraemaeker 2017, Kong *et al.* 2017a, Liu *et al.* 2017, Zou *et al.* 2015). In these applications, a common structural form is the longitudinally sandwiched piezoelectric transducers that often generate and receive waves in a single direction (Arnold *et al.* 2012, Lin and Xu 2008, Lin and Xu 2018, Lin *et al.* 2019, Zhang and Shi 2011, Zhang *et al.* 2019).

On the other hand, cylindrical piezoelectric transducers have been developed to generate and receive two-dimensional waves in the radial direction (Aronov 2009, Ebenezer 2004, Gao *et al.* 2018a, b, Kim and Lee 2007, Lin and Wang 2011, Wang and Shi 2013, Zhang and Shi 2010). In comparison with these two forms of transducer, piezoelectric spherical transducers (Alkoy *et al.* 1997, Alkoy *et al.* 1999, Kim *et al.* 2004, Kim *et al.* 2005, Kong *et al.* 2017a) can realize the generation and reception of omni-directional waves due to the characteristic of spherical configuration, and have attracted extensive attention (Alkoy *et al.* 2009, George *et al.* 2010, Kong *et al.* 2017b, Qin 2010, Wang *et al.* 2015).

In the literature, two main techniques have been reported to fabricate piezoelectric spherical transducers. One is the coaxial nozzle slurry process technique. Alkoy *et al.* (Alkoy *et al.* 1997, Alkoy *et al.* 1999, Alkoy *et al.* 2009) successfully fabricated a kind of BB transducers with several millimeters in diameter. These transducers can work at the order of kHz and MHz omnidirectional response, which have been used in ultrasonic imaging and hydrophones applications (Alkoy *et al.* 1999, Alkoy *et al.* 2009, Meyer *et al.* 2001). The other is the conventional technique that bonds two hemispheres using the adhesive agent to form a whole sphere. Kim *et al.* (2004) fabricated a single layer piezoelectric spherical transducer by bonding two hemispherical shells. In order to connect the inner electrodes, a hole in one shell was designed to thread the wire. Qin (2010) proposed and developed a piezoelectric shell

\*Corresponding author, Ph.D., Professor

E-mail: GSong@UH.EDU

\*\* Ph.D.

E-mail: jianjunwang168@ustb.edu.cn

transducer with stacked configuration, in which two radially polarized spherical piezoceramic shells are connected mechanically in series using the epoxy resin and electrically in parallel using wires. Each spherical piezoceramic shell is also made of two hemispherical shells. This new configuration can obtain both the omni-directionality and the high transmitting power, which is suitable for underwater acoustic detection. In the field of civil engineering, Kong *et al.* (Kong *et al.* 2017b, Kong *et al.* 2017a) developed a kind of spherical smart aggregate (SSA). Its core component is a spherical piezoceramic shell with radial polarization direction. In addition, an ultra-high performance concrete (UHPC) case is designed to protect the piezoceramic shell and ensure the compatibility with concrete matrix materials and durability under overloaded situation. The SSA possesses not only outstanding omnidirectional actuating and sensing capabilities but also good embeddability and compatibility with concrete structures, and thus has promising application in civil structural health monitoring.

To assist the design and fabrication of the devices, many theoretical efforts have been made on modeling and characterizing the dynamic behavior of various piezoelectric spherical structures, aiming at providing guidance in the design of such transducers. Various methods and analytical tools have been developed to deal with the complex electromechanical coupling problem in the piezoelectric spherical structures, including the discrete-layer model (Heyliger and Wu 1999), the improved orthogonal polynomial approach (Yu *et al.* 2013), the finite element formulation (Ramirez and Buchanan 2004), the polynomial expansion method (PEM) (Loza and Shul'Ga 1984), the method based on Bessel functions and Frobenius power series (George *et al.* 2010, Li *et al.* 2001), the simplified method that neglects the effect of the terms including  $e_{31}$  (Kim *et al.* 2005), the state-space approach (Chen 2001, Hasheminejad and Gudarzi 2015), and the matrix Frobenius power-series method (FPSM) (Chen 2000). Recently, on the basis of these methods, Wang *et al.* (Wang *et al.* 2018b, Wang *et al.* 2018a) developed an improved method based on several special functions to investigate the dynamic characteristics of the BB transducers, the stacked piezoceramic shell transducers, the SSA and the general multilayer transducers. The aim was to comprehensively understand the performance of these devices and to establish the appropriate design foundation to promote their further development and application.

The earlier investigations have shown that the selection of piezoelectric material types and variation of the geometrical dimensions will significantly affect the dynamic characteristics of these spherical transducers. However, once the transducer is fabricated, it is difficult to change these factors. As a result, the transducer only has the fixed prescribed dynamic characteristics. Challenge appears when they are utilized in applications with special requirement for multi-frequency or frequency varying scenarios. Therefore, an alternative design of such spherical transducers with broad band or tunability of dynamic characteristics is highly demanded. In the previous attempts to improve the longitudinally sandwiched piezoelectric transducers, the cylindrical piezoelectric transducers and the cymbal transducers, a variety of strategies have been explored to obtain the multi-frequency dynamic characteristics of these transducers, such as inductive matching

circuit regulation (Lin and Xu 2017, Lin 2017), external resistance tuning (Lin 2004, Wang *et al.* 2017, Wang *et al.* 2018c), coupling vibration mode excitation (Lin 2007), pre-stress control (Arnold and Mühlen 2001), elastic foundation stiffness variation (Wang and Luo 2016), and transformation temperature control of nitinol end caps with superelastic and shape-memory effects (Feeney and Lucas 2014, 2016, 2018). Among these methods, the resistance tuning method is the easiest way to effectively achieve the multi-frequency dynamic characteristics, and has been successfully applied to adjustable solid conical-type and step-type longitudinal ultrasonic horns (Lin *et al.* 2018, Tian *et al.* 2018). This method is yet to be applied to design the spherical piezoelectric transducers. To this end, this paper proposes an improved design with the resistance tuning strategy, and investigates their dynamic characteristics through analytical, numerical and experimental studies.

The remaining contents of this work are organized as follows. Section 2 introduces the proposed improved design of the piezoelectric spherical transducers, and presents the basic equations of the spherically symmetric piezoceramic shell and epoxy resin in such transducers. Section 3 derives the theoretical solution of the proposed transducers based on our previous work. Section 4 performs the numerical analysis to discuss influences of the resistance, the middle surface radius and the thickness of the epoxy adhesive layer on the dynamic characteristics. Section 5 presents the model validation by comparing the derived solution with literature given several special examples, followed by an experimental study. Section 6 concludes the paper.

## 2. Basic equations

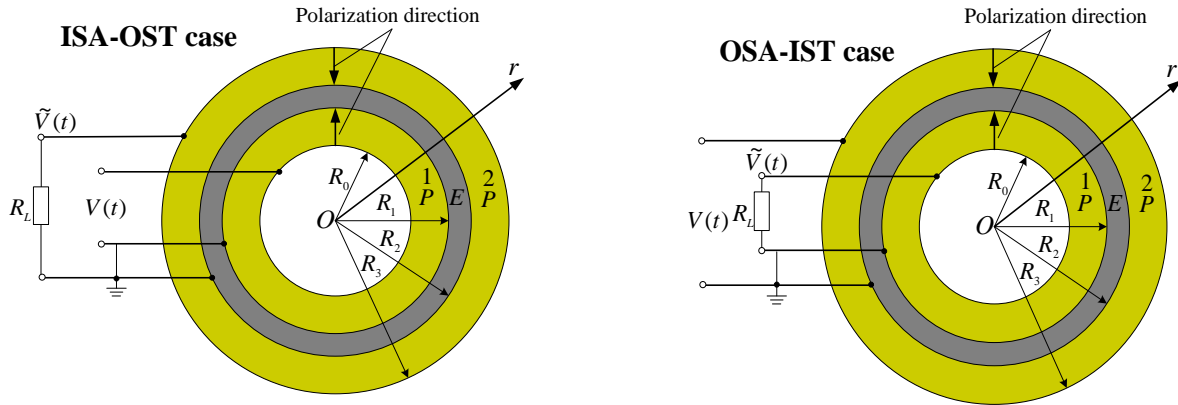
As shown in Fig. 1, a type of improved piezoelectric spherical transducer using the resistance tuning method is illustrated, which is developed from our previous work (Wang *et al.* 2018b) in which all the piezoelectric layers are connected in parallel electrically. The transducer includes two typical cases. The first one is that the inner shell for actuation and the outer shell for tuning (ISA-OST). The second one is opposite to the first case that is the outer shell for actuation and the inner shell for tuning (OSA-IST). Two shells are polarized along  $r$ -axis. Symbols  $P$  and  $E$  in Fig. 1 denote the piezoceramic shell and the epoxy resin, respectively. The thicknesses of the epoxy adhesive layer and the piezoceramic shell are  $t_E = (R_2 - R_1)$  and  $t_P = (R_1 - R_0) = (R_3 - R_2)$ , respectively. In addition, the middle surface radius is  $R_{middle} = R_0 + t_P + t_E/2$ .

Considering the harmonic motion, the applied voltage in the actuating shell and the generated voltage in the tuning shell are assumed as

$$V(t) = V_0 e^{j\omega t} \quad (1)$$

$$\tilde{V}(t) = \tilde{V}_0 e^{j\omega t} \quad (2)$$

where  $V_0$ ,  $\omega = 2\pi f$  and  $f$  are the amplitude, angular frequency and frequency of actuating voltage  $\tilde{V}_0$  is the



(a) The inner shell for actuation and the outer shell for tuning (ISA-OST)

(b) The outer shell for actuation while the inner shell for tuning (OSA-IST)

Fig. 1 Improved design of piezoelectric spherical transducers

complex amplitude of the generated voltage.  $j = \sqrt{-1}$  is the imaginary unit. Similar to the previous work (Wang *et al.* 2018b), the radial displacement  $u_{rPi}$ , stress  $\sigma_{rPi}$ , electric potential  $\phi_i$  and electric displacement  $D_{ri}$  of spherically symmetric piezoceramic shell are as follows (Wang *et al.* 2018b)

$$u_{rPi} = [A_{Pi}f_1(r) + B_{Pi}f_2(r) + \alpha(i)C_{li}f_3(r)]e^{j\omega t} \quad (3)$$

$$\sigma_{rPi} = [A_{Pi}f_4(r) + B_{Pi}f_5(r) + \alpha(i)C_{li}f_6(r)]e^{j\omega t} \quad (4)$$

$$\phi_i = [A_{Pi}\alpha(i)f_7(r) + B_{Pi}\alpha(i)f_8(r) + C_{li}f_9(r) + C_{0i}]e^{j\omega t} \quad (5)$$

$$D_{ri} = \frac{C_{li}}{r^2} e^{j\omega t} \quad (6)$$

In Eqs. (3)-(6),  $i=1,2$ ,  $\alpha(i) = (-1)^{i+1}$ , the known functions  $f_1(r) \sim f_9(r)$  were defined by Eqs. (35)-(43) in Appendix 1 of the earlier work (Wang *et al.* 2018b).  $A_{Pi}$ ,  $B_{Pi}$ ,  $C_{li}$  and  $C_{0i}$  are the undetermined coefficients.

For the spherically symmetric epoxy resin, the harmonic radial displacement  $u_{rE}$  and stress  $\sigma_{rE}$  are as follows (Wang *et al.* 2018b)

$$u_{rE} = [A_E f_{10}(r) + B_E f_{11}(r)]e^{j\omega t} \quad (7)$$

$$\sigma_{rE} = [A_E f_{12}(r) + B_E f_{13}(r)]e^{j\omega t} \quad (8)$$

where the known functions  $f_{10}(r) \sim f_{13}(r)$  were defined by Eqs. (44)-(47) in Appendix 1 of the earlier work (Wang *et al.* 2018b).  $A_E$  and  $B_E$  are the undetermined coefficients.

### 3. Theoretical solution

In this section, the above basic equations will employed

to derive the solution of the improved design by combining boundary conditions and continuous conditions, which are as follows

$$\sigma_{rP1}|_{r=R_0} = 0 \quad (9)$$

$$\begin{cases} \phi_1|_{r=R_0} = V(t) \text{ (for ISA-OST case)} \\ \phi_1|_{r=R_0} = \tilde{V}(t) = R_L \tilde{I}(t) = -R_L d\left(\int_{S_0} D_{r1}|_{r=R_0} dS_0\right)/dt \\ \quad = -j\omega 4\pi R_L C_{11} e^{j\omega t} = \tilde{V}_0 e^{j\omega t} \text{ (for OSA-IST case)} \\ \phi_1|_{r=R_1} = 0 \end{cases} \quad (10)$$

$$\begin{cases} u_{rE}|_{r=R_1} = u_{rP1}|_{r=R_1} \\ \sigma_{rE}|_{r=R_1} = \sigma_{rP1}|_{r=R_1} \\ u_{rP2}|_{r=R_2} = u_{rE}|_{r=R_2} \\ \sigma_{rP2}|_{r=R_2} = \sigma_{rE}|_{r=R_2} \end{cases} \quad (11)$$

$$\begin{cases} \phi_2|_{r=R_2} = 0 \\ \phi_2|_{r=R_3} = \tilde{V}(t) = R_L \tilde{I}(t) = R_L d\left(\int_{S_3} D_{r2}|_{r=R_3} dS_3\right)/dt \\ \quad = j\omega 4\pi R_L C_{12} e^{j\omega t} = \tilde{V}_0 e^{j\omega t} \text{ (for ISA-OST case)} \\ \phi_2|_{r=R_3} = V(t) \text{ (for OSA-IST case)} \end{cases} \quad (12)$$

$$\sigma_{rP2}|_{r=R_3} = 0 \quad (13)$$

In Eqs. (10) and (12),  $\tilde{I}(t)$  is the current across the resistance  $R_L$ .  $\tilde{V}_0 = j\omega 4\pi R_L C_{12}$  (for ISA-OST case) or  $\tilde{V}_0 = -j\omega 4\pi R_L C_{11}$  (for OSA-IST case) is the complex amplitude of the generated voltage.  $S_0$  and  $S_3$  are the spherical surface areas at  $r = R_0$  and  $r = R_3$ , respectively.

Substituting Eqs. (3)-(8) into Eqs. (9)-(13), a linear algebraic equations can be given as

$$\delta_{kl} \tilde{M} = \tilde{N} V_0 \quad (14)$$

Here,  $\delta_{kl}$  ( $k=l=10$ ),  $\tilde{M}$  and  $\tilde{N}$  are the matrices, as follows

$$\delta_{kl} = \begin{bmatrix} \delta_{11} & \delta_{12} & \cdots & \delta_{1l} \\ \delta_{21} & \delta_{22} & \cdots & \delta_{2l} \\ \cdots & \cdots & \cdots & \cdots \\ \delta_{k1} & \delta_{k2} & \cdots & \delta_{kl} \end{bmatrix} \quad (15)$$

where

$$\delta_{11} = f_4(R_0), \delta_{12} = f_5(R_0), \delta_{13} = f_6(R_0) \quad (16)$$

$$\delta_{21} = f_7(R_0), \delta_{22} = f_8(R_0), \delta_{23} = \begin{cases} f_9(R_0) & \text{(ISA-OST case)} \\ f_9(R_0) + j\omega 4\pi R_L & \text{(OSA-IST case)} \end{cases}, \delta_{24} = 1 \quad (17)$$

$$\delta_{31} = f_7(R_1), \delta_{32} = f_8(R_1), \delta_{33} = f_9(R_1), \delta_{34} = 1 \quad (18)$$

$$\delta_{41} = f_1(R_1), \delta_{42} = f_2(R_1), \delta_{43} = f_3(R_1), \delta_{45} = -f_{10}(R_1), \delta_{46} = -f_{11}(R_1) \quad (19)$$

$$\delta_{51} = f_4(R_1), \delta_{52} = f_5(R_1), \delta_{53} = f_6(R_1), \delta_{55} = -f_{12}(R_1), \delta_{56} = -f_{13}(R_1) \quad (20)$$

$$\delta_{65} = f_{10}(R_2), \delta_{66} = f_{11}(R_2), \delta_{67} = -f_1(R_2), \delta_{68} = -f_2(R_2), \delta_{69} = f_3(R_2) \quad (21)$$

$$\delta_{75} = f_{12}(R_2), \delta_{76} = f_{13}(R_2), \delta_{77} = -f_4(R_2), \delta_{78} = -f_5(R_2), \delta_{79} = f_6(R_2) \quad (22)$$

$$\delta_{87} = -f_7(R_2), \delta_{88} = -f_8(R_2), \delta_{89} = f_9(R_2), \delta_{8(10)} = 1 \quad (23)$$

$$\delta_{97} = -f_7(R_3), \delta_{98} = -f_8(R_3), \delta_{99} = \begin{cases} f_9(R_3) - j\omega 4\pi R_L & \text{(ISA-OST case)} \\ f_9(R_3) & \text{(OSA-IST case)} \end{cases}, \delta_{9(10)} = 1 \quad (24)$$

$$\delta_{10(7)} = f_4(R_3), \delta_{10(8)} = f_5(R_3), \delta_{10(9)} = -f_6(R_3) \quad (25)$$

It should be noted that other unspecified coefficients in Eqs. (16)-(25) are zero, and the coefficients  $\delta_{23}$  and  $\delta_{99}$  are different for two cases.

$$\tilde{M} = [A_{P1} \ B_{P1} \ C_{11} \ C_{01} \ A_E \ B_E \ A_{P2} \ B_{P2} \ C_{12} \ C_{02}]^T \quad (26)$$

$$\tilde{N} = [0 \ \tilde{V}_1 \ 0 \ 0 \ 0 \ 0 \ 0 \ 0 \ \tilde{V}_2 \ 0]^T \quad (27)$$

where

$$\tilde{V}_1 = \begin{cases} 1, & \text{(for ISA-OST case)} \\ 0, & \text{(for OSA-IST case)} \end{cases} \quad (28)$$

$$\tilde{V}_2 = \begin{cases} 0, & \text{(for ISA-OST case)} \\ 1, & \text{(for OSA-IST case)} \end{cases} \quad (29)$$

Solving Eq. (14), the coefficients  $A_{P1}$ ,  $B_{P1}$ ,  $C_{11}$ ,  $C_{01}$ ,  $A_E$ ,  $B_E$ ,  $A_{P2}$ ,  $B_{P2}$ ,  $C_{12}$  and  $C_{02}$  can be obtained.

$$\tilde{M}(n) = \chi_n V_0 \quad (n=1, 2, \dots, 10) \quad (30)$$

where  $\tilde{M}(1) = A_{P1}$ ,  $\tilde{M}(2) = B_{P1}$ ,  $\tilde{M}(3) = C_{11}$ , and so on.  $[\chi_1 \ \chi_2 \ \chi_3 \ \chi_4 \ \chi_5 \ \chi_6 \ \chi_7 \ \chi_8 \ \chi_9 \ \chi_{10}]^T = (\delta_{kl})^{-1} \tilde{N}$ . The input electrical impedance  $Z$  is then given as

$$Z = \begin{cases} V(t)/I_1(t) = 1/(j\omega 4\pi \chi_3) & \text{(for ISA-OST case)} \\ V(t)/I_2(t) = 1/(-j\omega 4\pi \chi_9) & \text{(for OSA-IST case)} \end{cases} \quad (31)$$

Here, the input currents  $I_1(t)$  and  $I_2(t)$  can be obtained through the derivative of the input electrical charge.

$$I_1(t) = \frac{d(\int_{S_0} D_{r1}|_{r=R_0} dS_0)}{dt} = j\omega 4\pi \chi_3 V_0 e^{j\omega t} \quad (32)$$

(for ISA-OST case)

$$I_2(t) = -\frac{d(\int_{S_3} D_{r2}|_{r=R_3} dS_3)}{dt} = -j\omega 4\pi \chi_9 V_0 e^{j\omega t} \quad (33)$$

(for OSA-IST case)

Subsequently, the resonance and anti-resonance frequencies  $f_r$  and  $f_a$  can be solved by taking  $|Z| = |Z|_{\min}$  and  $|Z| = |Z|_{\max}$ , respectively. The electromechanical coupling coefficient of the transducer is defined as (Mason 1950)

$$k_d^2 = \frac{f_a^2 - f_r^2}{f_a^2} \quad (34)$$

#### 4. Analysis and discussion

In this section, numerical analysis is performed to discuss the effect of the tuning resistance on the dynamic characteristics. PZT-4 is selected as piezoceramic material, and its material parameters are listed in Table 1. The material parameters of epoxy resin are as follows: Young's modulus  $E_E = 3.89 \times 10^9 \text{ N/m}^2$ , Poisson's ratio  $\nu_E = 0.38$ , density  $\rho_E = 1200 \text{ kg/m}^3$ . The geometric dimensions of the transducer are given as:  $t_P = 0.8 \text{ mm}$ ,  $t_E = 0.1 \text{ mm}$ ,  $R_{\text{middle}} = 12.7 \text{ mm}, 14.5 \text{ mm}, 20 \text{ mm}$ ,  $R_0 = R_{\text{middle}} - (t_P + t_E/2)$ ,  $R_1 = R_0 + t_P$ ,  $R_2 = R_1 + t_E$ , and  $R_3 = R_2 + t_P$ .

Figs. 2-4 show the fundamental resonance and anti-resonance frequencies  $f_r$  and  $f_a$ , as well as the fundamental electromechanical coupling coefficient  $k_d$  versus the resistance  $R_L$ . It should be pointed that changing the

Table 1 Material parameters of PZT-4 (Lin *et al.* 2013) and BaTiO<sub>3</sub> (Hussein and Heyliger 1998)

Material types	Elastic constant ( $\times 10^{10}$ N/m <sup>2</sup> )				Piezoelectric constant (C/m <sup>2</sup> )		Dielectric constant	Density (kg/m <sup>3</sup> )
	$c_{11}^E$	$c_{12}^E$	$c_{13}^E$	$c_{33}^E$	$e_{31}$	$e_{33}$	$\kappa_{33}^E/\epsilon_0$	$\rho_p$
PZT-4	13.9	7.78	7.43	11.5	-5.2	15.1	635	7500
BaTiO <sub>3</sub>	15.0	6.60	6.60	14.6	-4.35	17.5	1700	5700

Note:  $\epsilon_0 = 8.85 \times 10^{-12}$  F/m, Permittivity of free space

Table 2 Comparisons of the fundamental  $f_r$  and  $f_a$  of two cases under the SC and OC conditions

$t_E$ (mm)	Case	EBC of the tuning element	$R_{middle}=12.7$ mm		$R_{middle}=14.5$ mm		$R_{middle}=20$ mm	
			$f_r$ (kHz)	$f_a$ (kHz)	$f_r$ (kHz)	$f_a$ (kHz)	$f_r$ (kHz)	$f_a$ (kHz)
0.1	ISA-OST	SC	79.83	83.19	69.89	72.82	50.63	52.75
		OC	83.03	86.55	72.7	75.78	52.68	54.9
	OSA-IST	SC	79.83	83.03	69.89	72.7	50.63	52.68
		OC	83.19	86.55	72.82	75.78	52.75	54.9
0	ISA-OST	SC	80.09	83.47	70.12	73.07	50.79	52.93
		OC	83.33	86.87	72.96	76.06	52.87	55.11
	OSA-IST	SC	80.09	83.33	70.12	72.96	50.79	52.87
		OC	83.47	86.87	73.07	76.06	52.93	55.11
Error(%)	ISA-OST	SC	0.33	0.34	0.33	0.34	0.32	0.34
		OC	0.36	0.37	0.36	0.37	0.36	0.38
	OSA-IST	SC	0.33	0.36	0.33	0.36	0.32	0.36
		OC	0.34	0.37	0.34	0.37	0.34	0.38

NOTE: Error = (No epoxy layer – Epoxy layer)/Epoxy layer

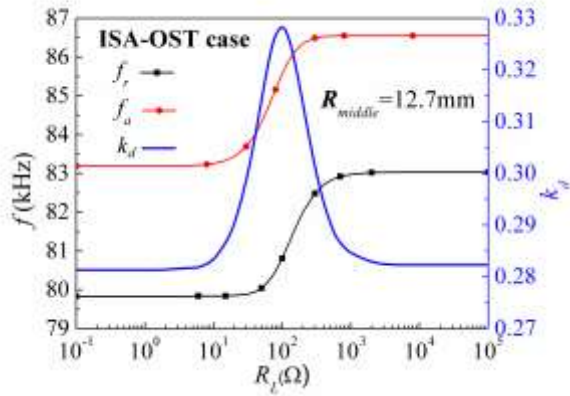
resistance from 0 to  $\infty$  induces the electrical boundary condition (EBC) shift from short circuit (SC) to open circuit(OC). In Figs. 2-4, the resistance range can approximately divide into non-sensitive range (NSR I) ( $R_L < 10^0 \Omega$ ), sensitive range (SR) ( $10^0 \Omega \leq R_L \leq 10^4 \Omega$ ) and NSR II ( $R_L > 10^4 \Omega$ ). The EBCs corresponding to the NSRs I and II can be approximately considered as the SC and OC states, respectively.

From Figs. 2-4, it can be observed that for both cases, the fundamental  $f_r$  and  $f_a$  shift from the SC frequencies to the OC ones when the resistance  $R_L$  increases, and the OC values are greater than the SC ones. Similar to the cylindrical composite transducers (Wang *et al.* 2017, Wang *et al.* 2018c), the physical explanations are as follow. Connecting different resistance to the tuning shell will enable its stiffness change, further affect the entire stiffness of the transducer. Different stiffness will generate different  $f_r$  and  $f_a$ . When the connecting resistance increases from 0 to  $\infty$ , the stiffness of the tuning shell shifts from the SC state to the OC state, further induces the related stiffness change of the transducer.

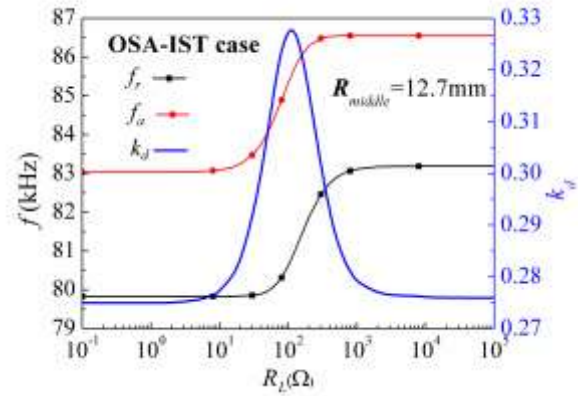
Furthermore, the fundamental  $f_r$  and  $f_a$  of two cases under the SC and OC EBCs are addressed in Table 2. It can be found that the SC  $f_r$  of ISA-OST case is equal to the SC  $f_r$  of OSA-IST case, while the SC  $f_a$  of ISA-OST case is equal to the OC  $f_r$  of OSA-IST case. The OC  $f_r$  of ISA-OST

case is equal to the SC  $f_a$  of OSA-IST case, while the OC  $f_a$  of ISA-OST case is equal to the OC  $f_a$  of OSA-IST case. This rule is similar to that of the resistance tuning cylindrical transducers (Wang *et al.* 2017, Wang *et al.* 2018c). The reason is that the EBCs corresponding to the  $f_r$  and  $f_a$  can be approximately considered as the SC and OC cases. Combining these cases as well as the SC and OC conditions determined by the resistance will generate these above special cases. A detailed working states analysis is presented in Table 3. It can be concluded that there exists a corresponding relationship between ISA-OST case and OSA-IST case for the SC and OC EBCs. Once the  $f_r$  and  $f_a$  of ISA-OST case are obtained, the corresponding frequencies of OSA-IST case can be determined. In addition, it also found that with the increase of the middle surface radius  $R_{middle}$ , the fundamental  $f_r$  and  $f_a$  present a decreasing trend.

From Figs. 2-4, it found that when the resistance increases, the fundamental  $k_d$  can reach to a maximum value at a special resistance. This special resistance is the matching resistance (Wang *et al.* 2018c), which can be selected to optimize the fundamental  $k_d$ . Furthermore, the matching resistance and the optimal fundamental  $k_d$  for different middle surface radius  $R_{middle}$  are addressed in Table 4. It showed that with the increase of the middle surface radius  $R_{middle}$ , the matching resistance is decreased; however, the optimal fundamental  $k_d$  is almost unaffected.

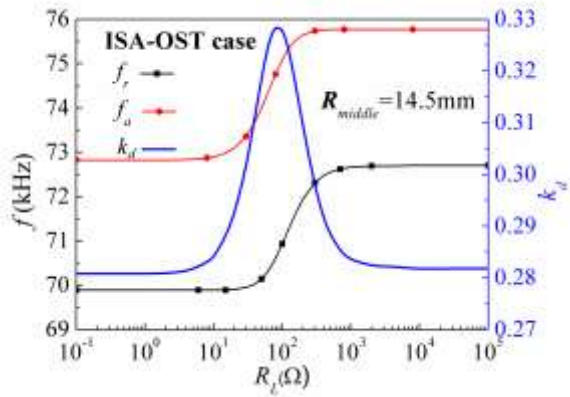


(a) ISA-OST case

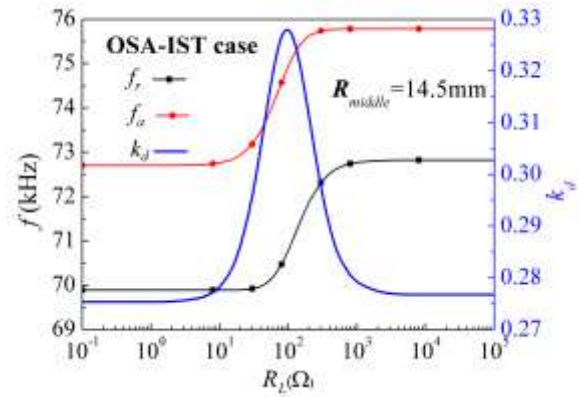


(b) OSA-IST case

Fig. 2 The fundamental  $f_r, f_a$  and  $k_d$  versus  $R_L$  for  $R_{middle}=12.7$  mm

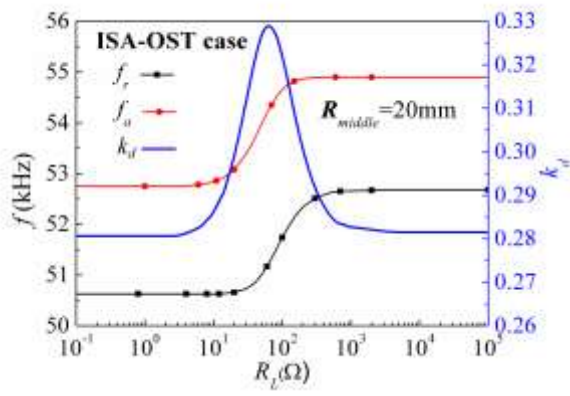


(a) ISA-OST case

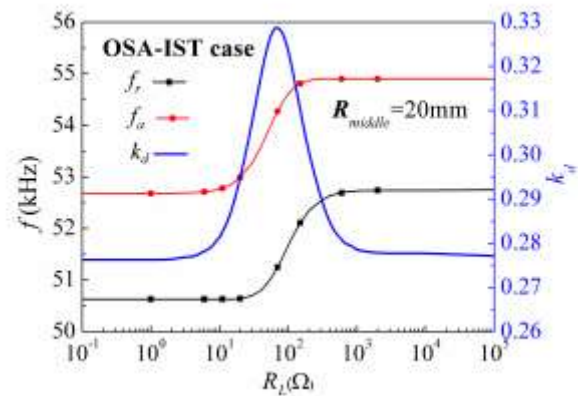


(b) OSA-IST case

Fig. 3 The fundamental  $f_r, f_a$  and  $k_d$  versus  $R_L$  for  $R_{middle}=14.5$  mm



(a) ISA-OST case



(b) OSA-IST case

Fig. 4 The fundamental  $f_r, f_a$  and  $k_d$  versus  $R_L$  for  $R_{middle}=20$  mm

In addition, in the practical situation, the epoxy adhesive layer is very thin, which can be neglected to simplify the problem. In order to prove the reasonability of this approach, the results of  $t_E = 0$ mm are also given in Table 2. The

maximum relative error for  $R_{middle} = 12.7$ mm, 14.5mm, 20mm is only 0.38%, validating the reliability of this simplification.

Table 3 Working states analysis of the special cases in Table 2

Case	EBC of the tuning element	EBC of the actuating element	
		Resonance	Anti-resonance
ISA-OST	(Outer shell) SC	(Inner shell) SC	(Inner shell) OC
	(Outer shell) OC	(Inner shell) SC	(Inner shell) OC
OSA-IST	(Inner shell) SC	(Outer shell) SC	(Outer shell) OC
	(Inner shell) OC	(Outer shell) SC	(Outer shell) OC

Table 4 The matching resistance and the optimal fundamental  $k_d$  for different middle surface radius  $R_{middle}$ 

Case	Optimal items	$R_{middle}=12.7$ mm	$R_{middle}=14.5$ mm	$R_{middle}=20$ mm
ISA-OST	Matching resistance ( $\Omega$ )	100	80	60
	Optimal fundamental $k_d$	0.3289	0.3285	0.3292
OSA-IST	Matching resistance ( $\Omega$ )	120	100	70
	Optimal fundamental $k_d$	0.3280	0.3285	0.3289

Table 5 The fundamental  $f_a$  obtained by the theoretical models in the present work and in Chen's work (Chen 2000) and Drenkow and Long's work (Drenkow and Long 1967)

No.	Model	$R_0$ (mm)	$R_1$ (mm)	$R_2$ (mm)	$R_3$ (mm)	$R_L$ ( $\Omega$ )	$f_a$ (kHz)
1	Chen (2000)	95	105	~	~	~	11.03
	Present (ISA-OST case)	95	105	105.01	105.02	$10^{10}$	11.024
	Present (OSA-IST case)	94.98	94.99	95	105	$10^{10}$	11.025
2	Drenkow and Long (1967)	95	105	~	~	~	12.446
	Present (ISA-OST case)	95	105	105.01	105.02	$10^{10}$	12.439
	Present (OSA-IST case)	94.98	94.99	95	105	$10^{10}$	12.441
3	Drenkow and Long (1967)	70	130	~	~	~	12.742
	Present (ISA-OST case)	70	130	130.01	130.02	$10^{10}$	12.748
	Present (OSA-IST case)	69.98	69.99	70	130	$10^{10}$	12.749

## 5. Validation

In this section, comparisons with several special examples in the earlier work are firstly performed to ensure the reliability of the derived solution. Subsequently, a prototype is fabricated to experimentally confirm the feasibility of the improved design.

### 5.1 Several special examples in the earlier work

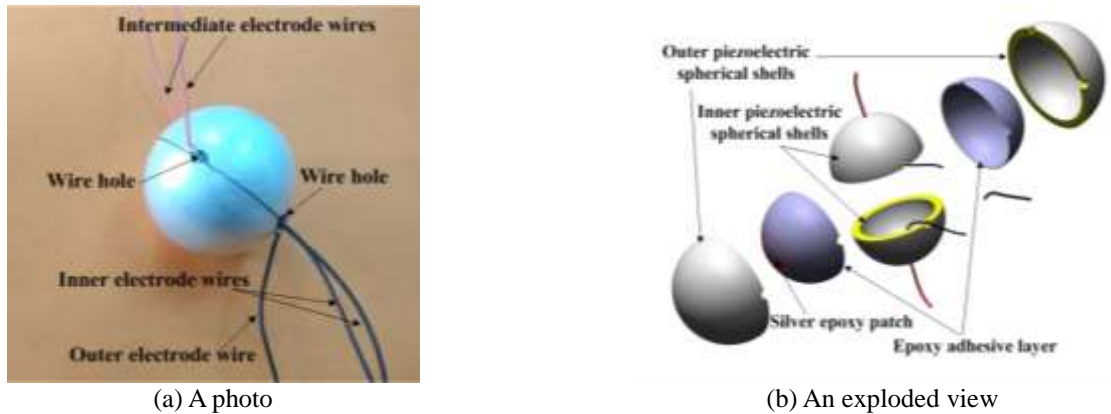
For comparisons, three examples are considered in Table 5. Example 1 is taken from Chen's work (Chen 2000), in which the free vibration of a spherically isotropic piezoelectric medium with radial inhomogeneity was investigated using the matrix FPSM. The inner and outer radii of the example 1 are respectively 95 mm and 105 mm, and PZT-4 listed in Table 1 is adopted. Examples 2 and 3 are taken from Drenkow and Long's work (Drenkow and Long 1967), in which the frequency equation for radial vibration of a BaTiO<sub>3</sub> sphere shell was established to solve the anti-resonance frequencies. Example 2 is that the inner

and outer radii are 95 mm and 105 mm, respectively. Example 3 is that the inner and outer radii are 70 mm and 130 mm, respectively. In these two examples, BaTiO<sub>3</sub> listed in Table 1 is adopted. The present models for ISA-OST case and OSA-IST case can be approximately reduced to these examples by taking the proper parameters, as listed in Table 5. Furthermore, the calculated fundamental anti-resonance frequencies are also listed in Table 5. The results obtained from the present model and the previous models are very close, validating the theoretical solution.

### 5.2 Experimental study

A prototype of the improved multi-frequency piezoelectric spherical transducer with  $R_{middle}=14.5$  mm is fabricated by using the conventional technique that bonds two hemispheres together using the adhesive agent to form a whole sphere, as shown in Fig. 5.

To clearly exhibit the schematic representation, a photo and an exploded view of the spherical transducer are presented. In the fabrication process, four hemispherical



(a) A photo

(b) An exploded view

Fig. 5 The fabricated improved piezoelectric spherical transducer



Fig. 6 Experimental setup

shells are prepared, including two identical inner shells with less radius and two identical outer shells with larger radius. Each inner shell has a wire hole for the electrical connection to the inner electrodes.

Two outer shells have respectively two wire holes along the two perpendicular radial directions to enable the electrical connection to the inner electrodes and the intermediate electrodes. A patch of silver epoxy is put between the inner and outer shells to connect electrically the intermediate electrodes between them. Two small shells are first glued together to form the inner whole sphere. Then, two large shells are coated to form the final transducer. Furthermore, the impedance spectra of the specimen are measured using an impedance analyzer (Agilent, model: 4294A), as shown in Fig. 6. A resistance control box (Shanghai Dongmao, model: ZX21f) with the range of 0-111.1110 M $\Omega$  is adopted to adjust the resistance value.

Figs. 7 and 8 plot the measured impedance spectra of two cases Fig. 9 further presents the corresponding measured  $f_r$  and  $f_a$  versus  $R_L$ . In addition, the theoretical results are also addressed in Figs. 7 and 8 for comparison. From these figures, it found that the measured and theoretical impedance spectra have a good agreement, and

the trend of the experimental  $f_r$  and  $f_a$  versus  $R_L$  is in general consistent with that from the theoretical prediction. Qualitatively, the theoretical  $f_r$  and  $f_a$  are larger than the measured results. The main reason is that the theoretical sphere shells are the perfect structures, while the actual shells are fabricated by the conventional fabrication technique that is bonding two hemispherical shells with wire holes to form a whole shell, which results in the decrease in the transducer stiffness. In addition, the possible minor difference between the real material parameters and the standard values adopted in the theory as well as the actual damping may also be the reasons for the difference in frequency. Furthermore, the experimental  $f_r$  and  $f_a$  of the SC and OC are compared with the theoretical values in Table 6 to further understand the discrepancy between them. In Table 6, the maximum relative error is 10.77%, validating basically the reliability of the theoretical predictions. However, the corresponding relationship between two cases for the SC and OC observed in the theory is not found in the experiment, which is also mainly caused by the above reasons.

From Fig. 9, it also observed that the  $f_r$  and  $f_a$  are relatively stable when  $R_L$  is larger than 200  $\Omega$ . That is because the electrical boundary conditions (EBCs)

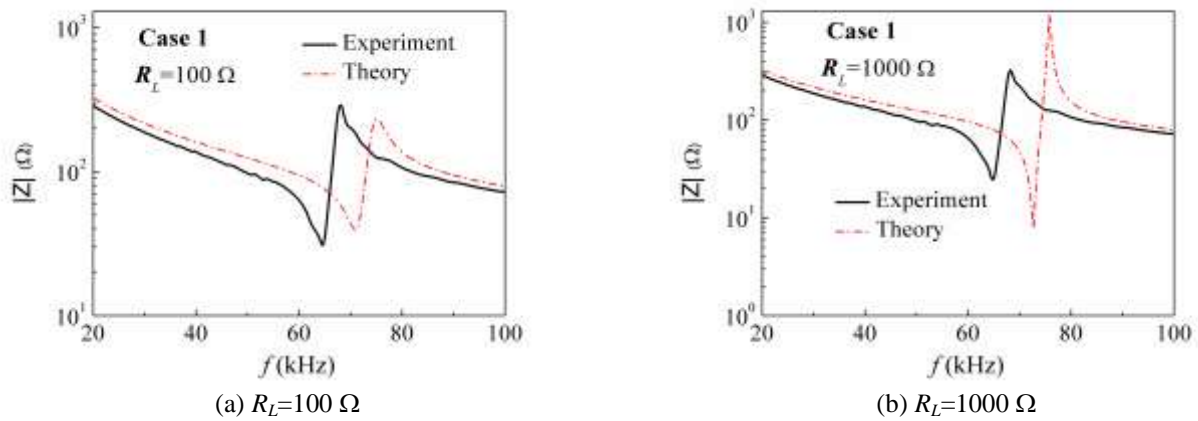


Fig. 7 Experimental and theoretical impedance spectra of ISA-OST case

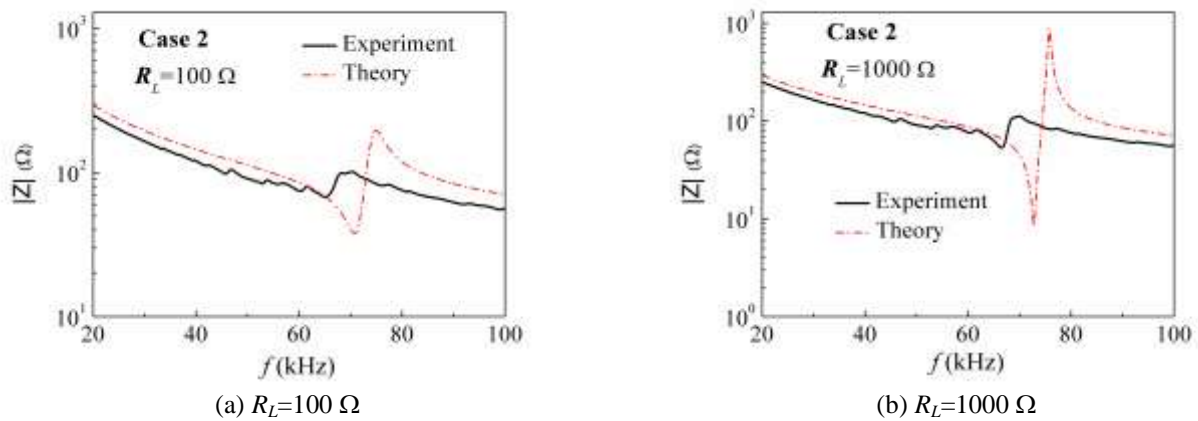


Fig. 8 Experimental and theoretical impedance spectra of OSA-IST case

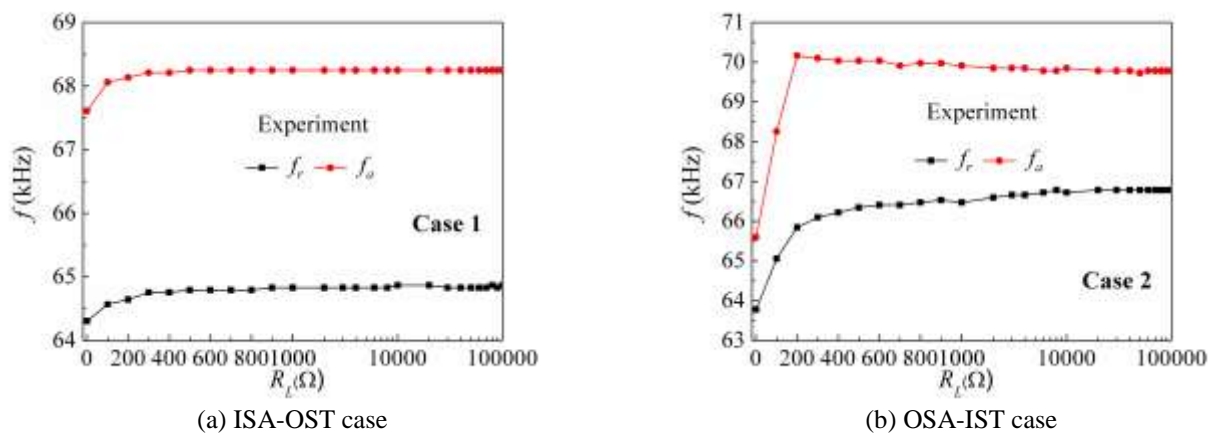


Fig. 9 The experimental  $f_r$  and  $f_a$  versus  $R_L$  for  $R_{middle}=14.5$  mm

corresponding to the states of  $R_L > 200 \Omega$  are the approximate open circuit (OC) cases. For these states, their  $f_r$  and  $f_a$  are relatively stable. This resistance range is also called the non-sensitive range (NSR) II. To achieve the multi-frequency characteristics, the resistance need be tuned

in the sensitive range (SR). In the experiential study, this resistance range is about  $0 > R_L > 200 \Omega$ . Although the range is relatively narrow, it proved the feasibility of this design. In the future study, the range can be widened by optimizing the geometric dimensions of the transducer.

Table 6 Comparisons of the fundamental  $f_r$  and  $f_a$  between experiment and theory for  $R_{middle}=14.5$  mm

Case	EBC of the tuning element	Experiment		Theory		Error(%)	
		$f_r$ (kHz)	$f_a$ (kHz)	$f_r$ (kHz)	$f_a$ (kHz)	$f_r$ (kHz)	$f_a$ (kHz)
ISA-OST	SC	64.31	67.61	69.89	72.82	7.98	7.15
	OC	64.87	68.25	72.7	75.78	10.77	9.94
OSA-IST	SC	63.78	65.59	69.89	72.7	8.74	9.78
	OC	66.78	69.79	72.82	75.78	8.29	7.90

NOTE: Error = (Theory – Experiment)/Theory

In general, although there are some difference between the experimental findings and theoretical results, the experimental findings still demonstrate the feasibility of this type of improved multi-frequency piezoelectric spherical transducers using the resistance tuning method, which have promising applications in extending the working frequencies range of the existing piezoelectric spherical transducer used in underwater acoustic detection, hydrophones, and the spherical smart aggregate (SSA) used in civil structural health monitoring. For example, the ISA-OST type and OSA-IST type SSAs can improve the efficiency of the active-sensing approach based on the traditional SSAs by virtue of their multiple resonance frequencies. In this method, an SSA actuator is used to generate the guided sinusoidal waves, and other SSA sensors are used to receive the signals. The guided sinusoidal waves can be a constant or sweep frequency. In order to receive the desirable signal responses, it is better to work near the resonance frequencies where the excited energy is larger than those of other ones. However, the traditional SSAs only have a single fixed frequency once they are fabricated. When this fixed frequency does not achieve the good effect, it will greatly weaken the performance of the method. The ISA-OST type and OSA-IST type SSAs show their potential ability in working multiple resonance frequencies, which is very helpful to provide a wide selection range to search an appropriate frequency that can greatly improve the efficiency and accuracy of this monitoring method.

In addition, in comparison to the existing piezoelectric spherical transducers with fixed prescribed dynamic characteristics, the advantages of the ISA-OST and OSA-IST transducers are that they can conveniently realize the multi-frequency characteristics by tuning the resistance, and can optimize the electromechanical coupling coefficient at the matching resistance. Their disadvantages are that the fabrication technique is relatively complex since it is needed to bond four hemispherical shells together and to design multiple appropriate wire holes to thread the inner electrodes. In comparison to the ISA-OST transducers, the OSA-IST transducers have the wider operating frequency range. The original reason came from the limit working states, as shown in Tables 2 and 3.

## 6. Conclusions

This work proposed a type of improved piezoelectric spherical transducers based on the resistance tuning method, and theoretically and experimentally investigated their dynamic characteristics. Compared to the existing piezoelectric spherical transducers, this improved design can conveniently realize the multi-frequency characteristics by tuning the resistance, and can obtain the maximum electromechanical coupling coefficient with a matching load resistance. In addition, there exists a corresponding relationship between ISA-OST case and OSA-IST case for the SC and OC EBCs of tuning shell. The proposed improved design has a great potential in benefitting the piezoelectric spherical transducers used in hydrophones, underwater acoustic detection and the piezoelectric elements of spherical smart aggregates (SSAs) used in civil structural health monitoring by extending their working frequencies range.

## Acknowledgments

The research described in this paper was financially supported in part by the National Natural Science Foundation of China (grant numbers 51708025, 61671068), in part by the Fundamental Research Funds for the Central Universities (grant number FRF-TP-19-023A2), and a doctoral student scholarship from the Chinese Scholarship Council (CSC).

## References

- Agrawal, B.N., Elshafei, M.A. and Song, G. (1997), "Adaptive antenna shape control using piezoelectric actuators", *Acta Astronautica*, **40**(11), 821-826. [https://doi.org/10.1016/S0094-5765\(97\)00185-9](https://doi.org/10.1016/S0094-5765(97)00185-9).
- Alkoy, S., Hladky, A.C., Dogan, A., Cochran Jr, J.K. and Newnham, R.E. (1999), "Piezoelectric hollow spheres for microprobe hydrophones", *Ferroelectrics*, **226**(1), 11-25. <https://doi.org/10.1080/00150199908230286>.
- Alkoy, S., Meyer Jr, R.J., Hughes, W.J., Cochran Jr, J.K. and Newnham, R.E. (2009), "Design, performance and modeling of piezoceramic hollow-sphere microprobe hydrophones", *Meas. Sci. Technol.*, **20**(9), 095204.
- Alkoy, S., Dogan, A., Hladky, A.C., Langlet, P., Cochran, J.K. and

- Newnham, R.E. (1997), "Miniature piezoelectric hollow sphere transducers (BBs)", *IEEE T. Ultrason. Ferr.*, **44**(5), 1067-1076. DOI: 10.1109/58.655632.
- Arnold, F.J. and Mühlen, S.S. (2001), "The mechanical pre-stressing in ultrasonic piezotransducers", *Ultrasonics*, **39**(1), 7-11. [https://doi.org/10.1016/S0041-624X\(00\)00048-2](https://doi.org/10.1016/S0041-624X(00)00048-2).
- Arnold, F.J., Bravo-Roger, L.L., Gonçalves, M.S. and Grilo, M. (2012), "Characterization of sandwiched piezoelectric transducers-a complement for teaching electric circuits", *Lat. Am. J. Phys. Educ.*, **6**(2), 216-220.
- Aronov, B.S. (2009), "Coupled vibration analysis of the thin-walled cylindrical piezoelectric ceramic transducers", *J. Acoust. Soc. Am.*, **125**(2), 803-818. <https://doi.org/10.1121/1.3056560>.
- Chen, W.Q. (2000), "Vibration theory of non-homogeneous, spherically isotropic piezoelectric bodies", *J. Sound Vib.*, **236**(5), 833-860. <https://doi.org/10.1006/jsvi.2000.3022>.
- Chen, W.Q. (2001), "Free vibration analysis of laminated piezoceramic hollow spheres", *J. Acoust. Soc. Am.*, **109**(1), 41-50. <https://doi.org/10.1121/1.1331110>.
- Drenkow, P.W. and Long, C.F. (1967), "Radial vibration of a thick-shell hollow piezoceramic sphere", *Acta Mech.*, **3**(1), 13-21. <https://doi.org/10.1007/BF01193597>.
- Dumoulin, C. and Deraemaeker, A. (2017), "Real-time fast ultrasonic monitoring of concrete cracking using embedded piezoelectric transducers", *Smart Mater. Struct.*, **26**(10), 104006.
- Du, G., Kong, Q., Wu, F., Ruan, J. and Song, G. (2016), "An experimental feasibility study of pipeline corrosion pit detection using a piezoceramic time reversal mirror", *Smart Mater. Struct.*, **25**(3), 037002.
- Du, G., Zhang, J., Zhang, J. and Song, G. (2017), "Experimental study on stress monitoring of sand-filled steel tube during impact using piezoceramic smart aggregates", *Sensors*, **17**(8), 1930. <https://doi.org/10.3390/s17081930>.
- Ebenezer, D.D. (2004), "Determination of complex coefficients of radially polarized piezoelectric ceramic cylindrical shells using thin shell theory", *IEEE T. Ultrason. Ferr.*, **51**(10), 1209-1215. DOI: 10.1109/TUFFC.2004.1350947.
- Feeney, A. and Lucas, M. (2014), "Smart cymbal transducers with nitinol end caps tunable to multiple operating frequencies", *IEEE T. Ultrason. Ferr.*, **61**(10), 1709-1719. DOI: 10.1109/TUFFC.2013.006231.
- Feeney, A. and Lucas, M. (2016), "Differential scanning calorimetry of superelastic Nitinol for tunable cymbal transducers", *J. Intel. Mat. Syst. Str.*, **27**(10), 1376-1387. <https://doi.org/10.1177/1045389X15591383>.
- Feeney, A. and Lucas, M. (2018), "A comparison of two configurations for a dual-resonance cymbal transducer", *IEEE T. Ultrason. Ferr.*, **65**(3), 489-496. DOI: 10.1109/TUFFC.2018.2793310.
- Feng, Q., Cui, J., Wang, Q., Fan, S. and Kong, Q. (2018), "A feasibility study on real-time evaluation of concrete surface crack repairing using embedded piezoceramic transducers", *Measurement*, **122**, 591-596. <https://doi.org/10.1016/j.measurement.2017.09.015>.
- Gao, W., Huo, L., Li, H. and Song, G. (2018a), "An embedded tubular PZT transducer based damage imaging method for two-dimensional concrete structures", *IEEE Access*, **6**, 30100-30109. DOI: 10.1109/ACCESS.2018.2843788.
- Gao, W., Huo, L., Li, H. and Song, G. (2018b), "Smart concrete slabs with embedded tubular PZT transducers for damage detection", *Smart Mater. Struct.*, **27**(2), 025002.
- George, J., Ebenezer, D.D. and Bhattacharyya, S.K. (2010), "Receiving sensitivity and transmitting voltage response of a fluid loaded spherical piezoelectric transducer with an elastic coating", *J. Acoust. Soc. Am.*, **128**(4), 1712-1720. <https://doi.org/10.1121/1.3478776>.
- Hasheminejad, S.M. and Gudarzi, M. (2015), "Active sound radiation control of a submerged piezocomposite hollow sphere", *J. Intel. Mat. Syst. Str.*, **26**(15), 2073-2091. <https://doi.org/10.1177/1045389X14549863>.
- Heyliger, P.R. and Wu, Y.C. (1999), "Electroelastic fields in layered piezoelectric spheres", *Int. J. Eng. Sci.*, **37**(2), 143-161. [https://doi.org/10.1016/S0020-7225\(98\)00068-8](https://doi.org/10.1016/S0020-7225(98)00068-8).
- Hou, S., Kong, Z., Wu, B. and Liu, L. (2018), "Compactness monitoring of compound concrete filled with demolished concrete lumps using PZT-based smart aggregates", *J. Aerosp. Eng.*, **31**(5), 04018064. [https://doi.org/10.1061/\(ASCE\)AS.1943-5525.0000903](https://doi.org/10.1061/(ASCE)AS.1943-5525.0000903).
- Hussein, M. and Heyliger, P. (1998), "Three-dimensional vibrations of layered piezoelectric cylinders", *J. Eng. Mech.*, **124**(11), 1294-1298. [https://doi.org/10.1061/\(ASCE\)0733-9399\(1998\)124:11\(1294\)](https://doi.org/10.1061/(ASCE)0733-9399(1998)124:11(1294)).
- Kim, J.O. and Lee, J.G. (2007), "Dynamic characteristics of piezoelectric cylindrical transducers with radial polarization", *J. Sound Vib.*, **300**(1-2), 241-249. <https://doi.org/10.1016/j.jsv.2006.08.021>.
- Kim, J.O., Hwang, K.K. and Jeong, H.G. (2004), "Radial vibration characteristics of piezoelectric cylindrical transducers", *J. Sound Vib.*, **276**(3-5), 1135-1144.
- Kim, J.O., Lee, J.G. and Chun, H.Y. (2005), "Radial vibration characteristics of spherical piezoelectric transducers", *Ultrasonics*, **43**(7), 531-537. <https://doi.org/10.1016/j.ultras.2005.01.004>.
- Kong, Q., Fan, S., Mo, Y.L. and Song, G. (2017a), "A novel embeddable spherical smart aggregate for structural health monitoring: Part II. numerical and experimental verifications", *Smart Mater. Struct.*, **26**(9), 095051.
- Kong, Q., Fan, S., Bai, X., Mo, Y.L. and Song, G. (2017b), "A novel embeddable spherical smart aggregate for structural health monitoring: Part I. fabrication and electrical characterization", *Smart Mater. Struct.*, **26**(9), 095050.
- Lewin, P.A. and Chivers, R.C. (1981), "Two miniature ceramic ultrasonic probes", *J. Phys. E: Sci. Instrum.*, **14**(12), 1420.
- Li, H., Liu, Z. and Lin, Q. (2001), "Spherical-symmetric steady-state response of fluid-filled laminate piezoelectric spherical shell under external excitation", *Acta Mech.*, **150**(1), 53-66. <https://doi.org/10.1007/BF01178544>.
- Li, W., Liu, T., Wang, J., Zou, D. and Gao, S. (2019), "Finite-element analysis of an electromechanical impedance-based corrosion sensor with experimental verification", *J. Aerosp. Eng.*, **32**(3), 04019012. [https://doi.org/10.1061/\(ASCE\)AS.1943-5525.0001002](https://doi.org/10.1061/(ASCE)AS.1943-5525.0001002).
- Lin, J., Lin, S. and Xu, J. (2019), "Analysis and experimental validation of longitudinally composite ultrasonic transducers", *J. Acoust. Soc. Am.*, **145**(1), 263-271. <https://doi.org/10.1121/1.5087554>.
- Lin, S. (2004), "Effect of electric load impedances on the performance of sandwich piezoelectric transducers", *IEEE T. Ultrason. Ferr.*, **51**(10), 1280-1286. DOI: 10.1109/TUFFC.2004.1350956.
- Lin, S. (2007), "Radial vibration of the composite ultrasonic transducer of piezoelectric and metal rings", *IEEE T. Ultrason. Ferr.*, **54**(6), 1276-1280. DOI: 10.1109/TUFFC.2007.381.
- Lin, S. (2017), "Study on the parallel electric matching of high power piezoelectric transducers", *Acta Acust. United Ac.*, **103**(3), 385-391. <https://doi.org/10.3813/AAA.919068>.
- Lin, S. and Xu, C. (2008), "Analysis of the sandwich ultrasonic transducer with two sets of piezoelectric elements", *Smart Mater. Struct.*, **17**(6), 065008.
- Lin, S. and Wang, S.J. (2011), "Radially composite piezoelectric ceramic tubular transducer in radial vibration", *IEEE T. Ultrason. Ferr.*, **58**(11), 2492-2498. DOI: 10.1109/TUFFC.2011.2106.

- Lin, S. and Xu, J. (2017), "Effect of the matching circuit on the electromechanical characteristics of sandwiched piezoelectric transducers", *Sensors*, **17**(2), 329. <https://doi.org/10.3390/s17020329>.
- Lin, S. and Xu, J. (2018), "Analysis on the cascade high power piezoelectric ultrasonic transducers", *Smart Struct. Syst.*, **21**(2), 151-161. <https://doi.org/10.12989/sss.2018.21.2.151>.
- Lin, S., Guo, H. and Xu, J. (2018), "Actively adjustable step-type ultrasonic horns in longitudinal vibration", *J. Sound Vib.*, **419**, 367-379. <https://doi.org/10.1016/j.jsv.2018.01.033>.
- Lin, S., Fu, Z.Q., Zhang, X.L., Wang, Y. and Hu, J. (2013), "Radially sandwiched cylindrical piezoelectric transducer", *Smart Mater. Struct.*, **22**(1), 015005.
- Liu, T., Zou, D., Du, C. and Wang, Y. (2017), "Influence of axial loads on the health monitoring of concrete structures using embedded piezoelectric transducers", *Struct. Health Monit.*, **16**(2), 202-214. <https://doi.org/10.1177/1475921716670573>.
- Liu, T., Huang, Y., Zou, D., Teng, J. and Li, B. (2013), "Exploratory study on water seepage monitoring of concrete structures using piezoceramic based smart aggregates", *Smart Mater. Struct.*, **22**(6), 065002.
- Luo, M., Li, W., Hei, C. and Song, G., (2016), "Concrete infill monitoring in concrete-filled FRP tubes using a PZT-based ultrasonic time-of-flight method", *Sensors*, **16**(12), 2083. <https://doi.org/10.3390/s16122083>.
- Loza, I.A. and Shul'Ga, N.A. (1984), "Axisymmetric vibrations of a hollow piezoceramic sphere with radial polarization", *Int. Appl. Mech.*, **20**(2), 113-117. <https://doi.org/10.1007/BF00883933>.
- Mason, W.P. (1950), *Piezoelectric crystals and their application to ultrasonics*, Van Nostrand Reinhold, New York.
- Meyer, J.L., Harrington, W.B., Agrawal, B.N. and Song, G., (1998), "Vibration suppression of a spacecraft flexible appendage using smart material", *Smart Mater. Struct.*, **7**(1), 95.
- Meyer, R., Newnham, R., Alkoy, S., Ritter, T. and Cochran, J. (2001), "Pre-focused lead titanate > 25 MHz single-element transducers from hollow spheres", *IEEE T. Ultrason. Ferr.*, **48**(2), 488-493. DOI: 10.1109/58.911731.
- Qin, L. (2010), Research on transducer with broad beamwidth, Ph.D. Thesis, Beijing University of Posts and Telecommunications, Beijing, China.
- Ramirez, G. and Buchanan, G. (2004), "Free vibrations of homogeneous and layered piezoelectric hollow spheres", *Int. J. Struct. Stab. Dy.*, **4**(3), 443-458. <https://doi.org/10.1142/S0219455404001318>.
- Tian, H., Lin, S. and Xu, J. (2018), "Longitudinally composite ultrasonic solid conical horns with adjustable vibrational performance", *Acta Acust. United Ac.*, **104**(1), 54-63. <https://doi.org/10.3813/AAA.919145>.
- Wang, H.M. and Luo, D.S. (2016), "Exact analysis of radial vibration of functionally graded piezoelectric ring transducers resting on elastic foundation", *Appl. Math. Model.*, **40**(4), 2549-2559. <https://doi.org/10.1016/j.apm.2015.09.108>.
- Wang, J.J. and Shi, Z.F. (2013), "Dynamic characteristics of an axially polarized multilayer piezoelectric/elastic composite cylindrical transducer", *IEEE T. Ultrason. Ferr.*, **60**(10), 2196-2203. DOI: 10.1109/TUFFC.2013.2810.
- Wang, J.J., Wei, P. and Ji, J. (2017), "Theoretical analysis of a resistance adjusting type piezoelectric cylindrical transducer", *J. Intel. Mat. Syst. Str.*, **28**(20), 2896-2907. <https://doi.org/10.1177/1045389X17704068>.
- Wang, J.J., Kong, Q., Shi, Z.F. and Song, G. (2018a), "A theoretical model for designing the novel embeddable spherical smart aggregate", *IEEE Access*, **6**, 48403-48417. DOI: 10.1109/ACCESS.2018.2851454.
- Wang, J.J., Wei, P., Qin, L. and Tang, L. (2018b), "Modeling and analysis of multilayer piezoelectric-elastic spherical transducers", *J. Intel. Mat. Syst. Str.*, **29**(11), 2437-2455. <https://doi.org/10.1177/1045389X18770868>.
- Wang, J.J., Qin, L., Song, W.B., Shi, Z.F. and Song, G. (2018c), "Electromechanical characteristics of radially layered piezoceramic/epoxy cylindrical composite transducers: theoretical solution, numerical simulation and experimental verification", *IEEE T. Ultrason. Ferr.*, **65**(9), 1643-1656. DOI: 10.1109/TUFFC.2018.2844881.
- Wang, L., Qin, L., Li, W., Zhang, B., Lu, Y. and Li, G. (2015), "Analysis on radial vibration of a stack of piezoelectric shells", *Ceram. Int.*, **41**(1), S856-S860. <https://doi.org/10.1016/j.ceramint.2015.03.159>.
- Xu, Y., Luo, M., Hei, C. and Song, G., (2018a), "Quantitative evaluation of compactness of concrete-filled fiber-reinforced polymer tubes using piezoceramic transducers and time difference of arrival", *Smart Mater. Struct.*, **27**(3), 035023.
- Xu, K., Deng, Q., Cai, L., Ho, S. and Song, G. (2018b), "Damage detection of a concrete column subject to blast loads using embedded piezoceramic transducers", *Sensors*, **18**(5), 1377. <https://doi.org/10.3390/s18051377>.
- Yu, J.G., Lefebvre, J.E. and Guo, Y.Q. (2013), "Wave propagation in multilayered piezoelectric spherical plates", *Acta Mech.*, **224**(7), 1335-1349. <https://doi.org/10.1007/s00707-013-0811-8>.
- Zhang, H., Hou, S. and Ou, J. (2018), "Smart aggregates for monitoring stress in structural lightweight concrete", *Measurement*, **122**, 257-263. <https://doi.org/10.1016/j.measurement.2018.03.041>.
- Zhang, T.T. and Shi, Z.F. (2010), "Exact analyses for two kinds of piezoelectric hollow cylinders with graded properties", *Smart Struct. Syst.*, **6**(8), 975-989. <http://dx.doi.org/10.12989/sss.2010.6.8.975>.
- Zhang, T.T. and Shi, Z.F. (2011), "Exact analysis of the dynamic properties of a 2-2 cement based piezoelectric transducer", *Smart Mater. Struct.*, **20**(8), 085017.
- Zhang, T.T., Zhang, K. and Liu, W. (2019), "Exact impact response of multi-layered cement-based piezoelectric composite considering electrode effect", *J. Intel. Mat. Syst. Str.*, **30**(3), 400-415. <https://doi.org/10.1177/1045389X18812713>.
- Zhu, J., Ho, S.C.M., Patil, D., Wang, N., Hirsch, R. and Song, G., (2017), "Underwater pipeline impact localization using piezoceramic transducers", *Smart Mater. Struct.*, **26**(10), p.107002.
- Zou, D., Liu, T., Huang, Y., Zhang, F., Du, C. and Li, B. (2014), "Feasibility of water seepage monitoring in concrete with embedded smart aggregates by P-wave travel time measurement", *Smart Mater. Struct.*, **23**(6), 067003.
- Zou, D., Liu, T., Liang, C., Huang, Y., Zhang, F. and Du, C. (2015), "An experimental investigation on the health monitoring of concrete structures using piezoelectric transducers at various environmental temperatures", *J. Intel. Mat. Syst. Str.*, **26**(8), 1028-1034. <https://doi.org/10.1177/1045389X14566525>.

BS